

$HZ\gamma$ production at 14 TeV LHC in next-to-leading order QCD

Xiong Shou-Jian^a, Ma Wen-Gan^a, Guo Lei^b, Zhang Ren-You^a, Chen Chong^a and Song Mao^c

^a Department of Modern Physics, University of Science and Technology of China,
Hefei, Anhui 230026, P.R.China

^b Department of Physics, Chongqing University, Chongqing 401331, P.R. China

^c School of Physics and Material Science, Anhui University, Hefei, Anhui 230039, P.R.China

January 28, 2022

Abstract

We investigate the process $pp \rightarrow HZ\gamma + X$ at the $\sqrt{s} = 14$ TeV LHC up to the QCD next-to-leading order (NLO), and discuss the kinematic distributions of final products after on-shell Higgs and Z -boson decays by adopting the narrow width approximation. The dependence of the leading order (LO) and the QCD NLO corrected integrated cross sections on the factorization/renormalization scale is studied. Our results show that the LO integrated cross section and kinematic distributions are significantly enhanced by the NLO QCD corrections, and the NLO QCD K -factor strongly depends on the observables and phase space. We conclude that in precision experimental data analyse for probing the $HZ\gamma$ coupling we should consider the NLO QCD corrections and put proper constraints on lepton-pair invariant mass to reduce the background.

PACS: 11.15.-q, 12.15.-y, 12.38.Bx

1 Introduction

In the standard model (SM) the Higgs boson serves for the breaking of the electroweak symmetry and the generation of the fundamental particle masses [1, 2]. Studying the Higgs mechanism is one of the main goals of the CERN Large Hadron Collider (LHC). In 2012 both the ATLAS and CMS collaborations announced the discovery of a new boson, whose properties are relatively close to the long awaited SM Higgs boson with mass of $m_H \sim 126$ GeV [3, 4]. After the discovery of the Higgs boson, the main task of further experiments is to determine its properties. Particularly, the precise determination of the Higgs boson couplings is imperative for verifying the validity of the SM and the existence of new physics at high energy scale.

The LHC first runs at 7 and 8 TeV are completed, and the latest data from them show that all the properties [5–9] of the new boson measured so far are well consistent with that of the SM Higgs boson, but it is well known that there are some theoretical difficulties associated with the SM Higgs sector. For example, the famous hierarchy problem, which is associated with the quadratic radiative corrections to the SM Higgs mass, is one of the difficulties, and there is no way to solve this problem in the SM. So new physics effects are still expected to solve these difficulties. There are many model candidates of new physics predicting sizeable deviations from the the Higgs couplings in the SM. In the SM some Higgs couplings of the types $g_{HVV'}$ and $g_{HVV'V''}$ are absent at the tree-level, and they would be particularly sensitive to new physics [10, 11]. With the increases of the LHC luminosity and colliding energy, we can collect statistically enough events for most of the important multi-body production processes. Obviously, precision measurements require accurate theoretical predictions for both signal and background. In the last few years, the phenomenological results including the next-to-leading order (NLO) QCD corrections to the Higgs boson production associated with di-gauge-boson at the LHC, such as $pp \rightarrow HWW$, $pp \rightarrow HW^\pm\gamma$, $pp \rightarrow HW^\pm Z$, have been studied [12–14].

The $HZ\gamma$ production at the LHC also offers the possibility to directly investigate the $HZ\gamma$, $HZZ\gamma$ and $HZ\gamma\gamma$ anomalous Higgs gauge couplings [15, 16], as they would cause deviations from the SM predictions. Moreover, an accurate estimate of the $pp \rightarrow HZ\gamma + X$ process followed with subsequent Higgs and Z -boson decays could provide the direct observable predictions in searching for possible new

physics. With the transverse momentum and rapidity cuts of $p_{T,cut}^\gamma = 5 \sim 20$ GeV and $y_{cut}^\gamma = 2.5$ on the final photon, the cross section for the $HZ\gamma$ production at the 14 TeV LHC is about $2.4 \sim 6.0$ fb, and therefore only about $170 \sim 420$ fb $^{-1}$ integrated luminosity is required to produce about 1000 events.

In this paper, we make a precision calculation for the $pp \rightarrow HZ\gamma + X$ process at the LHC including the NLO QCD corrections with on-shell Higgs and Z -boson decays in the narrow width approximation (NWA), but do not provide the detailed strategy to extract the information of the anomalous Higgs gauge couplings from the $pp \rightarrow HZ\gamma + X$ process. In section II we give the description of the analytical calculations for the LO cross section and the NLO QCD radiative corrections to the $pp \rightarrow HZ\gamma + X$ process. In section III we present some numerical results and discussions. Finally, a short summary is given.

2 Description of the computation

In this section we describe the analytical calculations at the LO and QCD NLO for the $pp \rightarrow HZ\gamma + X$ process.

A. LO calculation

In our calculations we employ FeynArts 3.4 package [17] to generate LO and QCD NLO Feynman diagrams and their corresponding amplitudes. The algebraic manipulations on the amplitudes are implemented by applying FormCalc 5.4 programs [18]. We neglect the masses of u -, d -, c -, s -quarks. Due to the smallness of (anti)bottom-quark density in proton, the LO contribution to the cross section from the $pp \rightarrow b\bar{b} \rightarrow HZ\gamma + X$ process at the 14 TeV LHC is less than 0.6%. Therefore, we do not consider the partonic process of $b\bar{b}$ annihilation in our calculations. Then the contributions to the cross section for the parent process $pp \rightarrow HZ\gamma + X$ come from the following partonic processes,

$$q(p_1) + \bar{q}(p_2) \rightarrow H(p_3) + Z(p_4) + \gamma(p_5), \quad (q = u, d, c, s), \quad (2.1)$$

where p_1 , p_2 and p_3 , p_4 , p_5 represent the four-momenta of the incoming partons and the outgoing H , Z and photon, respectively. The LO Feynman diagrams for the partonic process $q\bar{q} \rightarrow HZ\gamma$ are

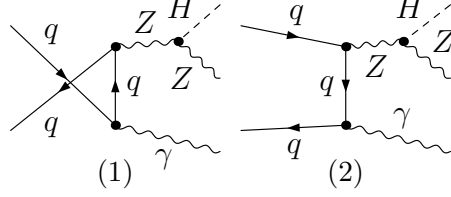


Figure 1: The LO Feynman diagrams for the partonic process $q\bar{q} \rightarrow HZ\gamma$.

shown in Fig.1. Since the Yukawa coupling strength is proportional to fermion mass and the u -, d -, c -, s -quarks are considered as massless, there is no contribution from the Feynman diagrams with internal Higgs boson line and the Higgs emission from initial quark. The LO amplitude for the $q\bar{q} \rightarrow HZ\gamma$ partonic process involves QED soft and collinear IR singularities since the photon is radiated from massless quark. To avoid these QED IR singularities and obtain an IR-safe LO result, we take the transverse momentum and rapidity cuts on the final photon ($p_{T,cut}^\gamma, |y_{cut}^\gamma|$) as declared in the following section. The LO matrix element for the partonic process $q\bar{q} \rightarrow HZ\gamma$ can be expressed as

$$\begin{aligned}
\mathcal{M}_{LO} &= \mathcal{M}_{LO}^u + \mathcal{M}_{LO}^t \\
&= \frac{ie^3 Q_q m_Z}{s_w^2 c_w^2} \bar{v}(p_2) \gamma^\mu (g_V^q - g_A^q \gamma^5) \frac{(\not{p}_1 - \not{p}_5)}{(p_1 - p_5)^2} \gamma^\nu u(p_1) \frac{1}{(p_3 + p_4)^2 - M_Z^2} \epsilon_\mu^*(p_4) \epsilon_\nu^*(p_5) \\
&+ \frac{ie^3 Q_q m_Z}{s_w^2 c_w^2} \bar{v}(p_2) \gamma^\nu \frac{(\not{p}_5 - \not{p}_2)}{(p_5 - p_2)^2} \gamma^\mu (g_V^q - g_A^q \gamma^5) u(p_1) \frac{1}{(p_3 + p_4)^2 - M_Z^2} \epsilon_\mu^*(p_4) \epsilon_\nu^*(p_5),
\end{aligned} \tag{2.2}$$

where $s_w = \sin \theta_W$, $c_w = \cos \theta_W$, $g_V^q = \frac{1}{2} T_q^3 - Q_q \sin^2 \theta_W$, $g_A^q = \frac{1}{2} T_q^3$, T_q^3 and Q_q are the third component of weak isospin and the electric charge of quark q separately.

The LO cross section for the partonic process $q\bar{q} \rightarrow HZ\gamma$ can be obtained by performing the integration over the phase space expressed as below,

$$\hat{\sigma}_{q\bar{q}}^0 = \frac{(2\pi)^4}{4|\vec{p}|\sqrt{s}} \int \overline{\sum} |\mathcal{M}_{LO}^{q\bar{q}}|^2 d\Omega_3, \tag{2.3}$$

where \vec{p} is the three-momentum of one initial parton in the center-of-mass system (c.m.s), \sqrt{s} is the colliding energy in partonic c.m.s, the summation is taken over the spins and colors of the initial and final states, and the bar over the summation indicates the averaging over the intrinsic degrees of

freedom of initial partons. $d\Omega_3$ is the three-body phase space element defined as

$$d\Omega_3 = \delta^{(4)} \left(p_1 + p_2 - \sum_{i=3}^5 p_i \right) \prod_{j=3}^5 \frac{d^3 \vec{p}_j}{(2\pi)^3 2E_j}. \quad (2.4)$$

By convoluting $\hat{\sigma}_{q\bar{q}}^0$ with the parton distribution functions (PDFs) of the colliding protons, we obtain the LO total cross section for the parent process $pp \rightarrow HZ\gamma + X$ as

$$\sigma_{LO} = \sum_q \int_0^1 dx_1 dx_2 \left[G_{q/P_1}(x_1, \mu_f) G_{\bar{q}/P_2}(x_2, \mu_f) \hat{\sigma}_{q\bar{q}}^0(\sqrt{\hat{s}} = x_1 x_2 \sqrt{s}) + (1 \leftrightarrow 2) \right], \quad (2.5)$$

where $G_{q/P}$ represents the PDF of parton q in proton P , x_i ($i = 1, 2$) describes the momentum fraction of a parton in proton, \sqrt{s} is the colliding energy in the rest frame of proton-proton system, and μ_f is the factorization scale.

B. NLO calculation

In the NLO calculations we use the dimensional regularization (DR) method in $D = 4 - 2\epsilon$ dimensions to regularize the ultraviolet (UV) and infrared (IR) divergences. The NLO QCD corrections to the $pp \rightarrow HZ\gamma + X$ process are constituted distinctly by the following three parts: (1) the virtual correction, (2) the real gluon and light-(anti)quark emission corrections, (3) the collinear counterterms of the PDFs. The virtual NLO QCD correction to the $q\bar{q} \rightarrow HZ\gamma$ partonic process consists of self-energy, vertex, box and counterterm diagrams. The one-loop Feynman diagrams are shown in Fig.2. We follow the definitions of tensor and scalar one-loop integral functions in Refs. [19, 20], and use the Passarino-Veltman (PV) method [19, 21] to reduce tensor integrals to the linear combinations of tensor structures and coefficients, where the tensor structures depend on the external momenta and the metric tensor, while the coefficients depend on scalar integrals and kinematic invariants. The whole reduction manipulations of a tensor integral to the lower-rank tensors and further to scalar integrals, is done and numerically calculated by using the LoopTools-2.2 library [18] and the FF package [22].

In the virtual correction calculation we need the wave function renormalization constants for quark fields. We introduce the renormalization constants $\delta Z_{\psi_{q,L,R}}$ for massless quark ($q = u, d, c, s$) fields defined as

$$\psi_{q,L,R}^0 = (1 + \delta Z_{\psi_{q,L,R}})^{1/2} \psi_{q,L,R}. \quad (2.6)$$

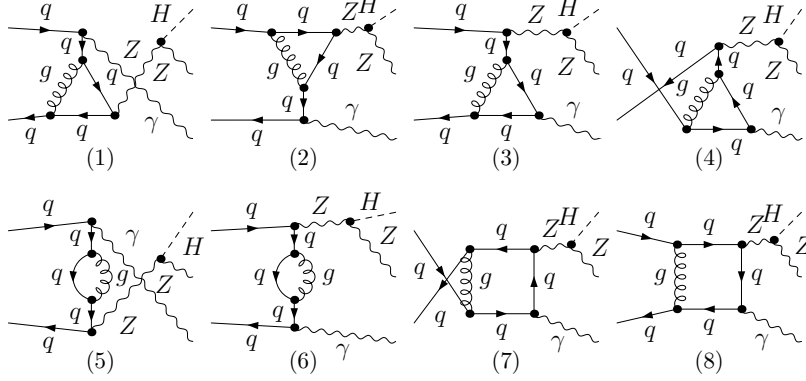


Figure 2: The one-loop Feynman diagrams for the partonic process $q\bar{q} \rightarrow HZ\gamma$.

In the modified minimal subtraction (\overline{MS}) renormalization scheme the renormalization constants for the massless quarks are expressed as

$$\delta Z_{\psi_{q,L}} = \delta Z_{\psi_{q,R}} = -\frac{\alpha_s}{4\pi} C_F (\Delta_{UV} - \Delta_{IR}), \quad (2.7)$$

where $C_F = 4/3$, $\Delta_{UV} = \frac{1}{\epsilon_{UV}} - \gamma_E + \ln(4\pi)$ and $\Delta_{IR} = \frac{1}{\epsilon_{IR}} - \gamma_E + \ln(4\pi)$.

After the reduction for tensor integrals, the amplitude for loop corrections involving one-loop scalar integrals contains both UV and IR divergences. The UV divergence is vanished after performing the renormalization procedure. But the total QCD NLO amplitude for the subprocess $q\bar{q} \rightarrow HZ\gamma$ still contains QCD soft/collinear IR singularities. We adopt the expressions in Ref. [23] to deal with the QCD IR divergences in Feynman integrals, and apply the expressions in Refs. [24–26] to implement the numerical evaluations for the QCD IR-finite parts of N -point scalar integrals. According to the Kinoshita-Lee-Nauenberg (KLN) theorem [27], these IR singularities will be cancelled by adding the contributions of the real gluon/light-(anti)quark emission subprocesses, and redefining the PDFs at the QCD NLO.

Since we put the transverse momentum, rapidity cuts on the final photon and a resolution cut on the photon and final jet throughout our LO and QCD NLO calculations, the numerical results for the real gluon/light-(anti)quark emission subprocesses are QED IR safe. While the real gluon/light-quark emission processes contain the QCD soft and collinear IR singularities. Technically, we isolate the QCD soft and collinear IR singularities by adopting the two cutoff phase space slicing (TCPSS)

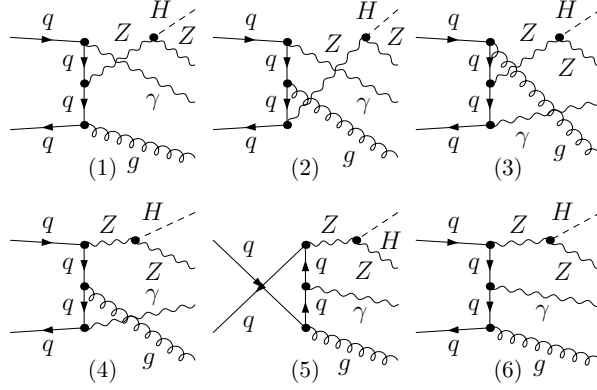


Figure 3: The Feynman diagrams for the real gluon emission subprocess $q\bar{q} \rightarrow HZ\gamma + g$.

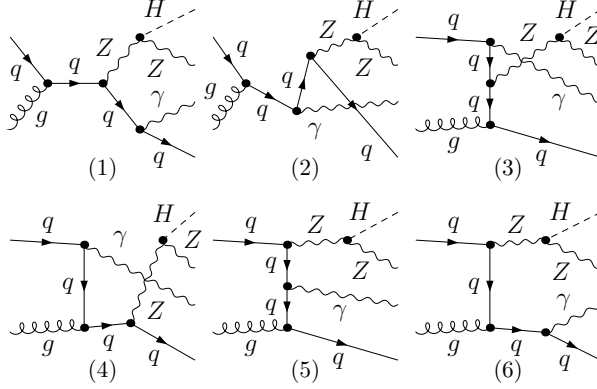


Figure 4: The Feynman diagrams for the real light-quark emission subprocess $qg \rightarrow HZ\gamma + q$.

method [28]. The Feynman diagrams for the real gluon and light-quark emission subprocesses are shown in Fig.3 and Fig.4, separately. Before our numerical calculations, we checked the UV and IR divergence cancelations both analytically and numerically. To verify the implementation of the TCPSS in right way, the independence of the NLO QCD corrected total cross section on the soft cutoff δ_s are checked in the range of $1 \times 10^{-5} < \delta_s < 1 \times 10^{-3}$ with $\delta_c = \delta_s/50$. In the further numerical calculations, we fix $\delta_s = 1 \times 10^{-3}$ and $\delta_c = 2 \times 10^{-5}$. Furthermore, we numerically compared our NLO QCD corrected cross sections with those obtained by using program MadGraph5_aMC@NLO of version 2.2.2 [29], and find they are in good agreement with each other within the Monte Carlo errors.

3 Results and discussions

In this section we present and discuss the numerical results for the $HZ\gamma$ associated production at the $\sqrt{s} = 14$ TeV LHC at both the LO and QCD NLO. We use the CTEQ6L1 and CT10nlo PDFs in the LO and NLO calculations, respectively. The strong coupling constant is determined by taking one-loop and two-loop running $\alpha_s(\mu)$ for the LO and NLO calculations separately, and setting the QCD parameter as $N_f = 5$, $\Lambda_5^{LO} = 165$ MeV for the CTEQ6L1 and $\Lambda_5^{\overline{MS}} = 226$ MeV for the CT10nlo. We set the factorization and renormalization scales to be equal, and take $\mu = \mu_f = \mu_r = \mu_0$ by default unless stated otherwise. The central scale is defined as $\mu_0 = E_T/2 = \frac{1}{2} \sum_i E_{T,i}$, where $E_{T,i} = \sqrt{p_{T,i}^2 + m_i^2}$ and the summation is taken over all the transverse energies of final particles. The related SM input parameters are taken as [3, 4, 30]

$$\alpha_{ew}^{-1} = 137.036, \quad m_W = 80.385 \text{ GeV}, \quad m_Z = 91.1876 \text{ GeV}, \quad m_H = 126 \text{ GeV}. \quad (3.1)$$

To strip the QED soft and collinear IR singularities at both the LO and QCD NLO, we put the following transverse momentum, rapidity and resolution cuts on the final photon, i.e.,

$$p_T^\gamma > p_{T,cut}^\gamma, \quad |y_\gamma| \leq |y_{cut}^\gamma| = 2.5, \quad (3.2)$$

$$R_{\gamma j} > \delta_0 \quad \text{or} \quad p_T^j \leq p_T^\gamma \frac{1 - \cos R_{\gamma j}}{1 - \cos \delta_0}. \quad (3.3)$$

where δ_0 is a fixed separation parameter which is set to be 0.7. The condition of Eq.(3.3) implies that the final jet can arbitrarily close to the photon as long as the jet is soft enough. In this way, we can preserve the full QCD singularities, which cancels against the virtual part, but it does not introduce divergence from the interaction between photon and massless quark-jet [31]. The limitation in Eq.(3.3) is to remove the QED collinear IR singularity due to a photon radiated from a final light-quark-jet j in the NLO calculation for the real light-quark emission processes. Then we accept the $HZ\gamma + jet$ events only if all the limitations in (3.2) and (3.3) are satisfied.

In Fig.5 we display the renormalization/factorization scale dependence of the LO, NLO QCD corrected total cross sections and the corresponding K -factor for the $pp \rightarrow HZ\gamma + X$ process at the $\sqrt{s} = 14$ TeV LHC by setting $\mu_r = \mu_f = \mu$. The LO and NLO QCD corrected integrated cross

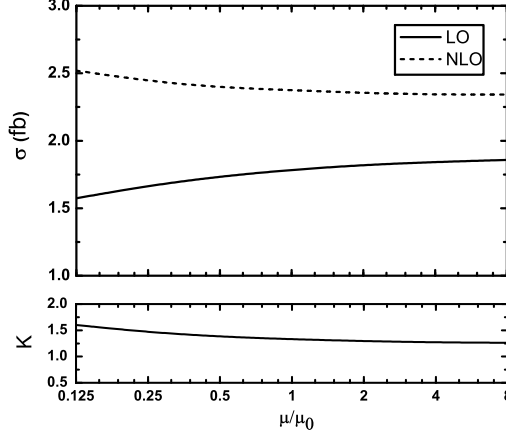


Figure 5: The dependence of the LO, NLO QCD corrected total cross sections and the corresponding K -factor for the $pp \rightarrow HZ\gamma + X$ process on the factorization/renormalization scale. Here we assume $\mu = \mu_r = \mu_f$ and define the central scale as $\mu_0 = E_T/2$.

$p_{T,cut}^\gamma$ (GeV)	σ_{LO} (fb)	σ_{NLO} (fb)	K
5	4.780(4)	5.99(3)	1.25
10	3.105(3)	4.01(2)	1.29
15	2.287(2)	3.00(1)	1.31
20	1.785(1)	2.37(1)	1.33

Table 1: The LO, NLO QCD corrected integrated cross sections and the corresponding K -factors with different cuts on p_T^γ for the $HZ\gamma$ production at the 14 TeV LHC.

sections are 1.785 fb and 2.37 fb, respectively, and the corresponding K -factor is 1.33 at the central scale $\mu = \mu_0$. If we defined the relative scale uncertainty as $\eta = [max(\sigma(\mu)) - min(\sigma(\mu))] / \sigma(\mu_0)$ with $\mu \in [0.25\mu_0, 4\mu_0]$, we get $\eta = 9.85\%$ and 4.24% for the LO and NLO QCD corrected cross sections, respectively. We can see that the dependence of the NLO QCD corrected total cross section on the factorization/renormalization scale is significantly reduced compared with that of the LO integrated cross section. This makes the theoretical predictions much more reliable.

We present the LO, NLO QCD corrected integrated cross sections and the corresponding K -factors for different cuts on p_T^γ in Tab.1. We can see that the LO and NLO QCD corrected total cross sections strongly depend on $p_{T,cut}^\gamma$, while the K -factor behaves not so sensitively to the cut. As shown in Tab.1, we can get a sizeable decrease in the total cross section with the increase of $p_{T,cut}^\gamma$ for the $pp \rightarrow HZ\gamma + X$

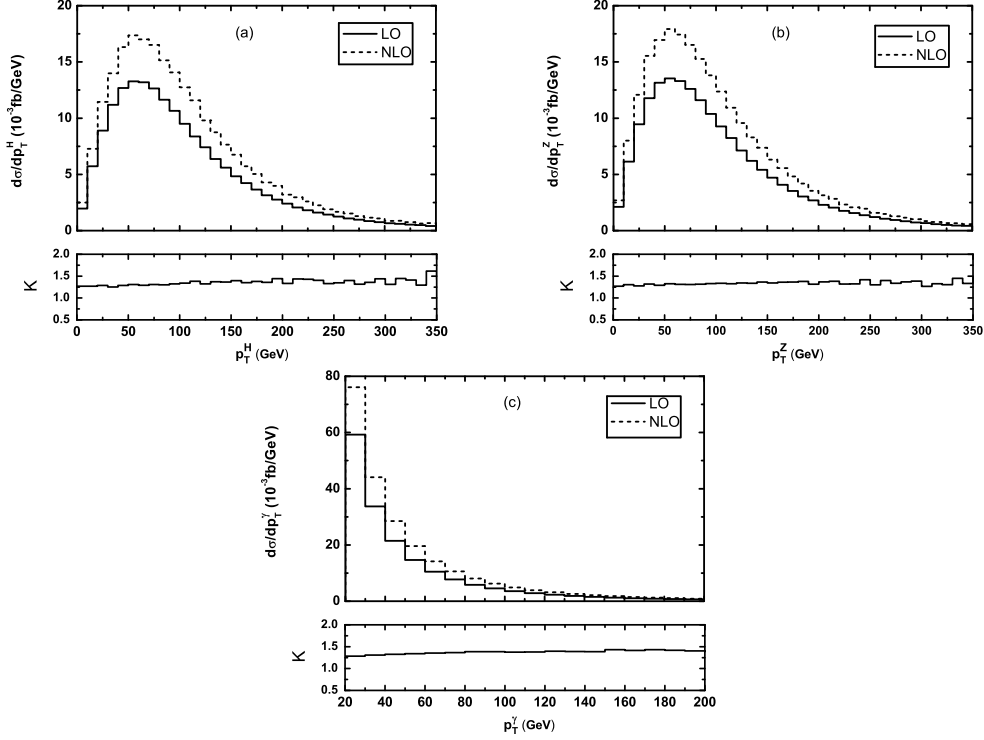


Figure 6: The LO, NLO QCD corrected transverse momentum distributions of the final particles and the corresponding K -factors for the $pp \rightarrow HZ\gamma + X$ process at the LHC. (a) p_T^H distributions, (b) p_T^Z distributions, (c) p_T^γ distributions.

process. In following numerical calculations we fix $p_{T,cut}^\gamma = 20$ GeV as the default choice.

We depict the LO, NLO QCD corrected distributions of the transverse momenta and the corresponding K -factors for the Higgs, Z -boson and photon produced by the $pp \rightarrow HZ\gamma + X$ process at the $\sqrt{s} = 14$ TeV LHC in Figs.6(a), (b) and (c), respectively. In Figs.6(a) and (b), the curves for $\frac{d\sigma}{dp_T^H}$ and $\frac{d\sigma}{dp_T^Z}$ at the LO and QCD NLO peak at the position of $p_T \sim 50$ GeV, and their K -factors are 1.31 and 1.33, respectively. Fig.6(c) shows that both the LO and NLO QCD corrected p_T^γ distributions decrease rapidly with the increase of the transverse momentum of photon. We can see from Figs.6(a,b,c) that the transverse momentum distributions for the Higgs, Z -boson and photon ($d\sigma_{LO}/dp_T^H$, $d\sigma_{LO}/dp_T^Z$, $d\sigma_{LO}/dp_T^\gamma$) are significantly enhanced by the NLO QCD corrections.

The final photon can be directly detected in experiment, while the produced on-shell Higgs and Z -boson are unstable particles and can be detected by their decay products. In order to investigate the kinematic distributions of final directly detected particles, we apply the NWA in analysing the

differential cross sections of the final Higgs and Z -boson decay products. We choose the Higgs boson decay channel of $H \rightarrow \tau^+\tau^-$ with $m_\tau = 1776.82$ MeV [30] and Z -boson decay channel of $Z \rightarrow \ell^+\ell^-$ ($\ell = e, \mu$) as the Higgs and Z -boson signals separately. By adopting HDECAY program [32] with input parameters from Ref. [30], we get $Br(H \rightarrow \tau^+\tau^-) = 5.897\%$, and take $Br(Z \rightarrow \ell^+\ell^-) = Br(Z \rightarrow e^+e^-) + Br(Z \rightarrow \mu^+\mu^-) = 3.363\% + 3.366\% = 6.729\%$ [30]. Then the signature for the $HZ\gamma$ production including the subsequent decays at the LHC can be written as

$$pp \rightarrow HZ\gamma \rightarrow \tau^+\tau^-\ell^+\ell^-\gamma + X \quad (\ell = e, \mu). \quad (3.4)$$

This signal is detected as an event including one τ -pair, one $e(\mu)$ -pair and a photon. For photon separation with other final particles in the rapidity-azimuthal angle plane, we impose the R cuts between photon and other final particles as below:

$$R_{\tau\gamma} > 0.4, \quad R_{l\gamma} > 0.4, \quad R_{j\gamma} > 0.7, \quad (3.5)$$

where $\ell = e, \mu$ and j denotes a jet with transverse momentum $p_T^j > 30$ GeV.

The final photon in the signal process $pp \rightarrow HZ\gamma \rightarrow \tau^+\tau^-\ell^+\ell^-\gamma$ ($\ell = e, \mu$) is only emitted from initial parton. However, the HZ associated production followed by the subsequent decays of $H \rightarrow \tau^+\tau^-\gamma$, $Z \rightarrow \ell^+\ell^-$ or $H \rightarrow \tau^+\tau^-$, $Z \rightarrow \ell^+\ell^-\gamma$ also leads to the $\tau^+\tau^-\ell^+\ell^-\gamma$ event and contributes at the same order as the signal process. This process, denoted as

$$pp \rightarrow HZ \rightarrow \tau^+\tau^-\ell^+\ell^-\gamma + X \quad (\ell = e, \mu), \quad (3.6)$$

is the main background in measuring the $HZ\gamma$ coupling via the $pp \rightarrow HZ\gamma \rightarrow \tau^+\tau^-\ell^+\ell^-\gamma + X$ process. We estimate the background process $pp \rightarrow HZ \rightarrow \tau^+\tau^-\ell^+\ell^-\gamma$ at the LO in the NWA by adopting CTEQ6L1 PDF, and take $\Gamma_Z = 2.4952$ GeV [30]. The total decay width of SM Higgs boson is obtained by using HDECAY program as $\Gamma_H = 4.38 \times 10^{-3}$ GeV. In analysing the $\tau^+\tau^-\ell^+\ell^-\gamma$ events, we adopt the event selection criteria shown in Eqs.(3.2) and (3.5), and impose the following invariant mass constraints on the final lepton pairs to suppress the background contribution:

$$\begin{aligned}
m_H - \Delta &< M_{\tau^+\tau^-} < m_H + \Delta, \\
m_Z - \Delta &< M_{\ell^+\ell^-} < m_Z + \Delta, \quad (\ell = e, \mu), \quad (\Delta = 5 \text{ or } 10 \text{ GeV}).
\end{aligned} \tag{3.7}$$

Then we obtain the background over signal as

$$\frac{\sigma_{LO}(pp \rightarrow HZ \rightarrow \tau^+\tau^-\ell^+\ell^-\gamma)}{\sigma_{LO}(pp \rightarrow HZ\gamma \rightarrow \tau^+\tau^-\ell^+\ell^-\gamma)} = \begin{cases} 8.1\%, & \Delta = 10 \text{ GeV} \\ 1.5\%, & \Delta = 5 \text{ GeV} \end{cases}. \tag{3.8}$$

Therefore, we can conclude that the background events with photon radiated from final charged leptons can be reduced distinctly in probing the $HZ\gamma$ coupling by taking proper invariant mass constraints on τ -pair and $e(\mu)$ -pair. In the following, we neglect the background contribution and only consider the signal process $pp \rightarrow HZ\gamma \rightarrow \tau^+\tau^-\ell^+\ell^-\gamma$ in investigating the kinematic distributions of the final produced leptons.

In Figs.7(a) and (c) we present the LO, NLO QCD corrected transverse momentum distributions of τ^+ and positively charged lepton ℓ^+ ($\ell = e, \mu$), and the corresponding K -factors at the $\sqrt{s} = 14$ TeV LHC, respectively. As shown in Figs.7(a) and (c), the QCD corrections always enhance the LO differential cross sections $d\sigma_{LO}/dp_T^{\tau^+}$ and $d\sigma_{LO}/dp_T^{\ell^+}$. Both the LO and NLO QCD corrected transverse momentum distributions of τ^+ and ℓ^+ reach their maxima at the positions of $p_T^{\tau^+} \sim 40$ GeV with $K = 1.31$ and $p_T^{\ell^+} \sim 30$ GeV with $K = 1.31$, respectively. Figs.7(b) and (d) are for the LO and NLO QCD corrected rapidity distributions of τ^+ and ℓ^+ separately. Both y^{τ^+} and y^{ℓ^+} reach their maxima at $y = 0$, with their K -factors being around 1.36. We can see from all these four figures that the NLO QCD corrections do not change the line-shapes of the transverse momentum and rapidity distributions, while enhance the LO differential cross sections significantly in all the plotted kinematic regions. With the transverse momentum and rapidity cuts of $p_{T,cut}^\gamma = 5 \sim 20$ GeV and $y_{cut}^\gamma = 2.5$ on the final photon, the accumulated luminosity of $1000 \sim 2660 \text{ fb}^{-1}$ is required to produce 25 $\tau^+\tau^-\ell^+\ell^-\gamma$ events via $pp \rightarrow HZ\gamma \rightarrow \tau^+\tau^-\ell^+\ell^-\gamma + X$ channel at the 14 TeV LHC.

4 Summary

In this paper we investigate the NLO QCD corrections to the $HZ\gamma$ production followed by subsequent Higgs and Z -boson decays at the $\sqrt{s} = 14$ TeV LHC. We study the dependence of the LO and NLO

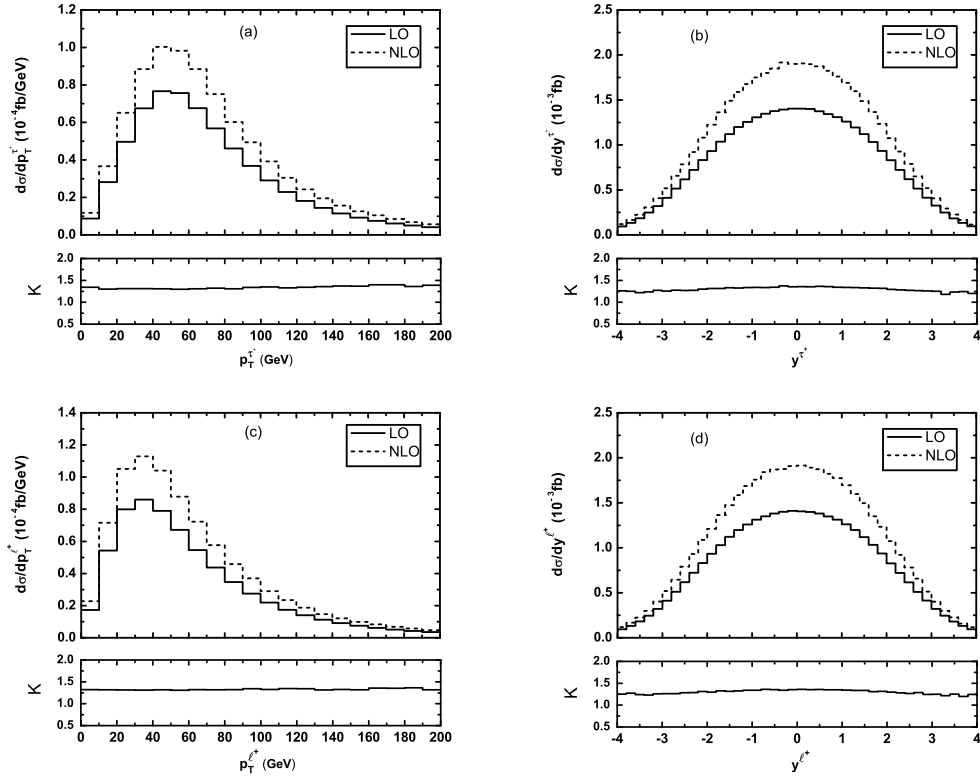


Figure 7: The LO, NLO QCD corrected transverse momentum and rapidity distributions of τ^+ and the positively charged lepton, and corresponding K -factors for the $pp \rightarrow HZ\gamma + X \rightarrow \tau^+\tau^-\ell^+\ell^-\gamma + X$ processes at the $\sqrt{s} = 14$ TeV LHC. (a) $p_T^{\tau^+}$ distributions, (b) y^{τ^+} distributions, (c) $p_T^{\ell^+}$ ($\ell = e, \mu$) distributions, (d) y^{ℓ^+} ($\ell = e, \mu$) distributions.

QCD corrected cross sections on the factorization/renormalization scale, and our results show that the scale uncertainty of the NLO QCD corrected cross section is reduced compared with that of the LO cross section. We present the LO and NLO QCD corrected distributions of transverse momenta and rapidities of the decay products of Higgs and Z -boson. We find that the NLO QCD radiative corrections are significant, and notably modify the LO kinematic distributions. We see also that the K -factor is distinctly related to phase space region and kinematic observable. We conclude that the NLO QCD corrections should be considered in precision experimental data analyse in measuring the $pp \rightarrow HZ\gamma + X$ process, and the background events with a photon radiated from final charged lepton can be reduced in probing the $HZ\gamma$ coupling by putting proper invariant mass constraints on final τ -pair and $e(\mu)$ -pair.

5 Acknowledgments

This work was supported in part by the National Natural Science Foundation of China (Grants. No.11275190, No.11375008, No.11375171).

References

- [1] S. L. Glashow, Nucl. Phys. **22**, 579 (1961); S. Weinberg, Phys. Rev. Lett. **19**, 1264 (1967); A. Salam, in Proceedings of the 8th Nobel Symposium, Stockholm, 1968, edited by N. Svartholm (Almquist and Wiksells, Stockholm, 1968), p. 367; H. D. Politzer, Phys. Rep. **14**, 129 (1974.)
- [2] P. W. Higgs, Phys. Lett. **12**, 132 (1964); Phys. Rev. Lett. **13**, 508 (1964); Phys. Rev. **145**, 1156 (1966); F. Englert and R. Brout, Phys. Rev. Lett. **13**, 321 (1964); G. S. Guralnik, C. R. Hagen and T. W. B. Kibble, Phys. Rev. Lett. **13**, 585 (1964); T. W. B. Kibble, Phys. Rev. **155**, 1554 (1967).
- [3] G. Aad *et al.* (ATLAS Collaboration), Phys. Lett. B **716**, 1 (2012).
- [4] S. Chatrchyan *et al.* (CMS Collaboration), Phys. Lett. B **716**, 30 (2012).
- [5] G. Aad *et al.* (ATLAS Collaboration), Phys. Rev. D **90**, 112015 (2014).

- [6] G. Aad *et al.* (ATLAS Collaboration), Phys. Rev. D **91**, 012006 (2015).
- [7] G. Aad *et al.* (ATLAS Collaboration), arXiv:1412.2641 [hep-ex] (2014).
- [8] V. Khachatryan *et al.* (CMS Collaboration), arXiv:1411.3441 [hep-ex] (2014).
- [9] V. Khachatryan *et al.* (CMS Collaboration), arXiv:1412.8662 [hep-ex] (2014).
- [10] G. Cacciapaglia, A. Deandrea, G. D. L. Rochelle and J-B. Flament, J. High Energy Phys. 03 (**2013**) 029.
- [11] J.-J. Cao, L. Wu, P.-W. Wu, and J.-M. Yang, J. High Energy Phys. 09 (**2013**) 043; C.-C. Han, N. Liu, L. Wu, J.-M. Yang and Y. Zhang, Eur. Phys. J. C **73**, 2664 (2013).
- [12] S. Mao, W.-G. Ma, R.-Y. Zhang, L. Guo, S.-M. Wang and L. Han, Phys. Rev. D **79**, 054016 (2009).
- [13] M. Song, N. Wan, G. Li, W.-G. Ma, R.-Y. Zhang, L. Guo, Y.-J. Zhou and J.-Y. Guo, Phys. Rev. D **88**, 076002 (2013).
- [14] N. Liu, J. Ren, L. Wu, P. Wu and J.-M. Yang, J. High Energy Phys. 04 (**2014**) 189.
- [15] M. C. Gonzalez-Garcia, Int. J. Mod. Phys. A **14**, 3121 (1999); M. Dubinin, H. J. Schreiber and A. Vologdin, Eur. Phys. J. C **30**, 337 (2003); S. D. Rindani and P. Sharma, Phys. Lett. B **693**, 134 (2010); A. Gutierrez-Rodriguez, J. Montano, and M. A. Perez, J. Phys. G **38**, 095003 (2011); M. B. Einhorn and J. Wudka, Nucl. Phys. **B877**, 792 (2013); H. Cai, J. High Energy Phys. 04 (**2014**) 052;
- [16] M. Baillargeon, F. Boudjema, F. Cuypers, E. Gabrielli, and B. Mele, Nucl. Phys. **B424**, 343 (1994).
- [17] T. Hahn, Comput. Phys. Commun. **140**, 418 (2001).
- [18] T. Hahn and M. Perez-Victoria, Comput. Phys. Commun. **118**, 153 (1999).
- [19] G. Passarino and M.J.G. Veltman, Nucl. Phys. **B160** 151 (1979).

- [20] A. Denner and S. Dittmaier, Nucl. Phys. **B734**, 62 (2006).
- [21] A. Denner, Fortsch. Phys. **41**, 307 (1993).
- [22] G. J. van Oldenborgh, NIKHEF-H/90-15.
- [23] R. K. Ellis and G. Zanderighi, J. High Energy Phys. 02, (**2008**) 002.
- [24] G.'t Hooft and M. Veltman, Nucl. Phys. **B153**, 365 (1979).
- [25] A. Denner, U. Nierste and R. Scharf, Nucl. Phys. **B367** 637 (1991).
- [26] A. Denner and S. Dittmaier, Nucl. Phys. **B658** 175 (2003).
- [27] T. Kinoshita, J. Math. Phys. (N.Y.) **3**, 650 (1962); T. D. Lee and M. Nauenberg, Phys. Rev. **133**, B1549 (1964).
- [28] B. W. Harris and J. F. Owens, Phys. Rev. **D65** 094032 (2002).
- [29] J. Alwall, M. Herquet, F. Maltoni, O. Mattelaer, T. Stelzer, JHEP 1106 **2011** 128.
- [30] J. Beringer *et al.* (Particle Data Group), Phys. Rev. D **86**, 010001 (2012).
- [31] S. Frixione, Phys. Lett. B **429**, 369 (1998).
- [32] A. Djouadi, J. Kalinowski, and M. Spira, Comput. Phys. Commun. 108, 56 (1998).